Available online at www.eccomasproceedia.org
Eccomas Proceedia COMPDYN (2017) 194-219

ECCOMAS
Proceedia

COMPDYN 2017
6th ECCOMAS Thematic Conference on
Computational Methods in Structural Dynamics and Earthquake Engineering
M. Papadrakakis, M. Fragiadakis (eds.)
Rhodes Island, Greece, 15–17 June 2017

IN-SITU MEASUREMENTS RELATED TO THE PERFORMANCE OF STONE MASONRY BRIDGES IN GREECE

G.C. Manos[1], E. Kozikopoulos[2], L. Kotoulas[3], N. Simos[3]

[1] Professor Emeritus and ex-Director of the Lab. of Strength of Materials and Structures, Aristotle University, Greece, e-mail: {gcmanos@civil.auth.gr}

[2] Ph.D. Canditate, Lab. of Strength of Materials and Structures, Aristotle University, Greece.
e-mail: {vago_kozi@outlook.com.gr}

[3] Ph.D. Canditate, Lab. of Strength of Materials and Structures, Aristotle University, Greece.
e-mail: {kotoulaslambros@gmail.com}

[4] Professional Engineer, Brookhaven National Laboratory, USA
e-mail: {simos@bnl.gov}

Keywords: Stone masonry bridges, Dynamic Measurements, Numerical Simulation, Foundation Deformability, Flooding, Damage from Explosion.

Abstract. *Stone masonry bridges are studied as part of the built cultural heritage, utilizing in-situ measurements in order to identify their dynamic characteristics in terms of eigen-frequencies, eigen-modes and damping properties. Such information is a valuable basis for building realistic numerical simulations of the structural behaviour of such bridges as well as for their structural health monitoring. Such simplified numerical analyses yielded numerical predictions of bridge deformations and stresses that are useful in understanding the structural behaviour and the structural damage potential for such masonry structures. The structural performance of Plaka bridge that collapsed due to flooding in February 2015 was examined when subjected to the gravitational forces combined with either simplified flooding loads or a design earthquake. Moreover, the structural damage that this bridge sustained during an explosion in 1944, was also examined combined with the flooding loads. It is shown that the flexibility of the foundation, amplified by long or short term erosion of the bridge-footings, results in a more detrimental response for the Plaka bridge, in terms of tensile stress fields, than the applied simplified flooding loads. The obtained numerical predictions demonstrate that the structural damaged sustained by this bridge during the 1944 explosion leads to a dominant tensile stress field at the regions of the main and secondary arches on top of the mid-pier. These predicted peak tensile stress values are well beyond the stone masonry strength. Consequently, they could well have contributed towards the 2nd of February 2015 collapse. Finally, simplified numerical simulations of the earthquake vulnerability for the Plaka bridge indicate that had this bridge not collapsed from flooding the design earthquake would have most probably led to its structural damage and its partial collapse.*

Peer-review under responsibility of the organizing committee of COMPDYN 2017.
doi: 10.7712/120117.5416.16895

1 INTRODUCTION

In what follows selective results are presented from an extensive study, which focused on old stone masonry bridges that are located mainly in the prefectures of Western Macedonia and Ipiros in Greece ([1], [2] , [3] and [27]). These bridges are examples of outstanding stone-masonry construction that was dominant for a long period in these parts of Greece. The old stone masonry bridges that survive today have been built during the 18th and 19th century. They were used to connect villages located in rough mountainous terrain bridging currents that could be quite turbulent during part of the year. This type of transporting people, animals and goods was accomplished using a relatively narrow deck with width varying from 2.0m to 3.0m. On the contrary, their size spans from 8m to 40m when a single arch is employed (Konitsa) or over 70m for multi-arch structures. More information on the geometry, construction characteristics and mechanical properties of the employed materials are given by Manos et al. (2016) [1]. Today, these structures have retain but only a small part of this primary function, as new roads and bridges have been built to facilitate the contemporary transportation needs. Despite this fact they have recently attracted considerable attention as cultural heritage structures together with an effort to become parts of a network of mountain trails. Because a number of people use these structures as visitors a conservation effort was also initiated for their maintenance. Our study has also partly such an objective. That is to obtain information through in-situ instrumentation and measurements on the vibration characteristics of these structures at a given time in a health monitoring framework, as described in section 2. In addition, these in-situ measurements are complemented with a numerical investigation that has as first target to form realistic numerical simulations of such old stone masonry structures. Moreover, to employ next such realistic numerical simulations in order to assess the behaviour of these old stone masonry bridges to a combination of loads that include accidental actions, such as forces generated from earthquakes or flooding.

Figure 1. Instrumentation used in the old stone masonry bridge of Tsipiani on 12th December, 2015.

2 IN-SITU MEASUREMENTS OF THE DYNAMIC CHARACTERISTICS OF THE STUDIED STONE BRIDGES.

In measuring the dynamic response of all the studied stone bridges two types of excitation were mobilized. The first, namely ambient excitation, mobilized the wind, despite the variation of the wind velocity in amplitude and orientation during the various tests. Due to the topography of the areas where these stone bridge are located, usually a relatively narrow gorge, the orientation of the wind resulted in a considerable component perpendicular to the longitudinal bridge axis. This fact combined with the resistance offered to this wind component by the façade of each bridge produced sufficient excitation source resulting in small amplitude vibrations that could be recorded by the employed instrumentation. For this purpose, the employed SysCom tri-axial velocity sensors had a sensitivity of 0.001mm/sec and a SysCom data acquisition system with a sampling frequency of 400Hz (see figure 1).

All the obtained data were subsequently studied in the frequency domain through available FFT software [1], [4], [5]. This wind orientation relative to the geometry of each bridge structure coupled with the bridge stiffness properties could excite mainly the 1st symmetric out-of-plane eigen-modes. The variability of the wind orientation could also excite, although to a lesser extend, some of the other in-plane and out-of-plane eigen-modes. This process will be presented for the old masonry bridge of Tsipiani depicted in figure 2.

Figure 2. The studied old stone masonry bridge of Tsipiani on 12th December, 2015.

2.1 Wind excitation for the old masonry bridge of Tsipiani

The basic geometry and the outline of the structural formation of this stone masonry bridge is depicted in figure 3. The locations of the velocity sensors are also shown together with the notation used for the coordinate system. As can be seen in this figure the clear span of the main central arch is 26m with a height from the water surface to the top of the deck approximately 13.65m. The main arch is supported on the left side on a rock formation whereas on

the right side the main central arch is supported on a number of secondary arches. The direction that the wind excited this bridge is also indicated. As can be seen, due to the flexibility of these stone masonry bridges, the direction of the river flow and the formation of the gorges that are crossed, the wind excites these structures mainly in the out-of-plane (Vx) direction. Figure 4 depicts the out-of-plane velocity response of Tsipianis Bridge due to wind excitation, as it was recorded on 12th December 2015 from a sensor placed at the mid-span of the main central arch. Figure 5 depicts the fast Fourier transform (FFT) diagram in terms of FFT amplitude and frequency values (Hz) for the measured out-of-plane response of this bridge due to the wind excitation, shown in figure 4. The dominant frequency (having the maximum amplitude) in this FFT diagram has a value of 3.369Hz. As will be discussed in the next session (2.2) this dominant frequency represents the eigen frequency for the symmetric out-of-plane eigen-mode for this structure.

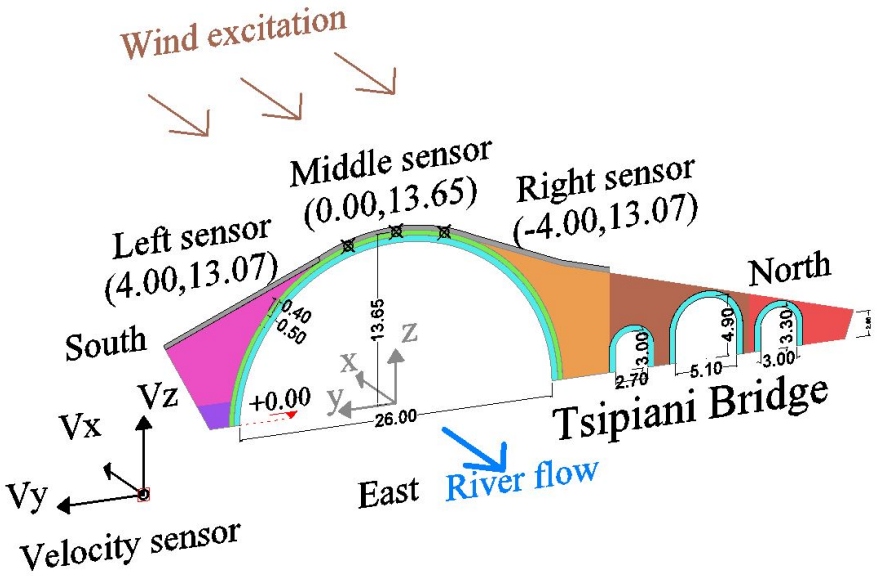

Fig. 3 Tsipianis Bridge, wind excitation

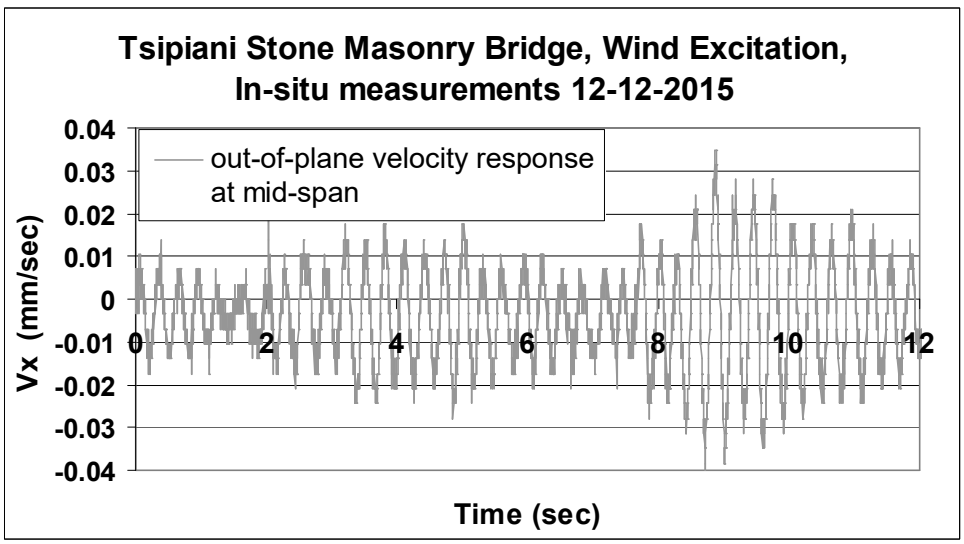

Fig. 4 Out-of-plane velocity response at mid-span of Tsipianis Bridge from wind excitation

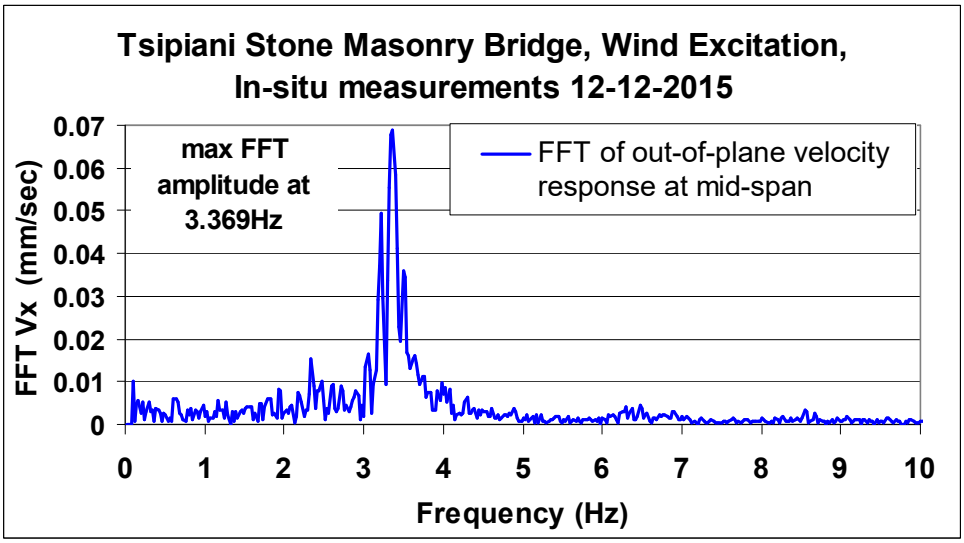

Fig. 5. Fast Fourier Transform diagram of the out-of-plane velocity response at mid-span of Tsipianis Bridge from wind excitation (shown in figure 4).

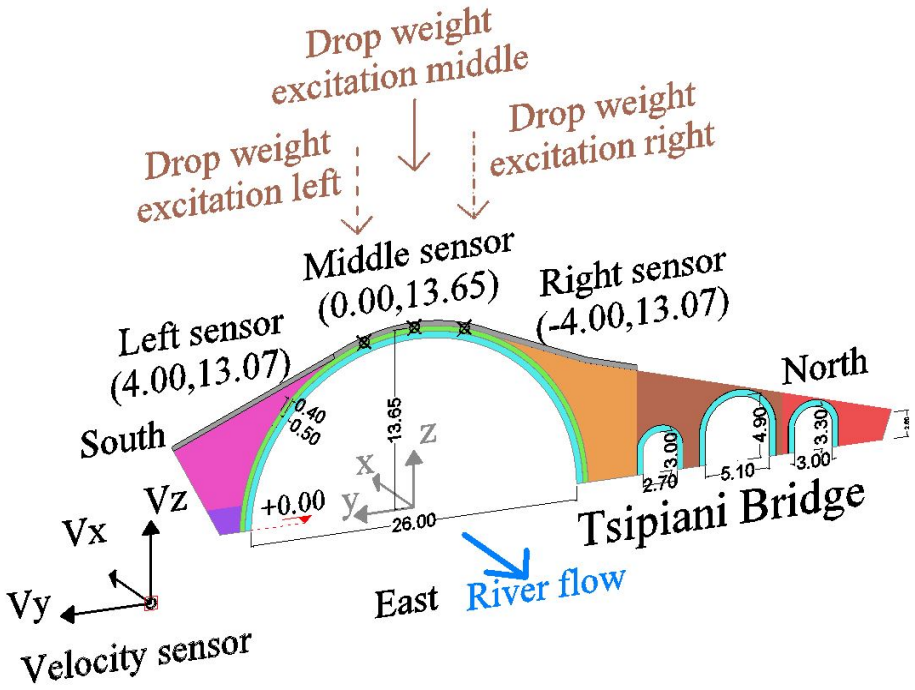

Figure 6. Tsipianis Bridge, drop weight excitation

2.2 Drop weight excitation for the old masonry bridge of Tsipiani

The second type of excitation that was employed, namely vertical in-plane excitation, was produced from a sudden drop of a weight on the deck (figure 6) of the stone masonry bridge [1], [6], [7]. This weight was of the order of approximately 2.0KN that was dropped from a relatively small height of 100mm, so as to avoid even the slightest damage to the stone surface of the deck of each bridge. Again the level of this second type of excitation was capable of producing mainly vertical vibrations and exciting the in-plane eigen-modes of each structure structures that could be capture by the employed SysCom tri-axial velocity sensors with a

sensitivity of 0.001mm/sec and a SysCom data acquisition system with a sampling frequency of 400Hz (see figure 1). All the obtained data were subsequently studied in the frequency domain through available FFT software. In figures 7a, 7c and 7e the velocity measurements are depicted along the three axes (Vx, x-x horizontal out-of-plane, Vy, y-y horizontal in-plane and Vz, in-plane z-z vertical) as they were recorded during a typical sampling with the drop weight excitation. In figure 7b, 7d and 7f the corresponding plots of the fast Fourier transforms in terms of FFT amplitudes of these velocity response measurements (Vx, x-x horizontal out-of-plane, Vy, y-y horizontal in-plane and Vz, in-plane z-z vertical) are shown.

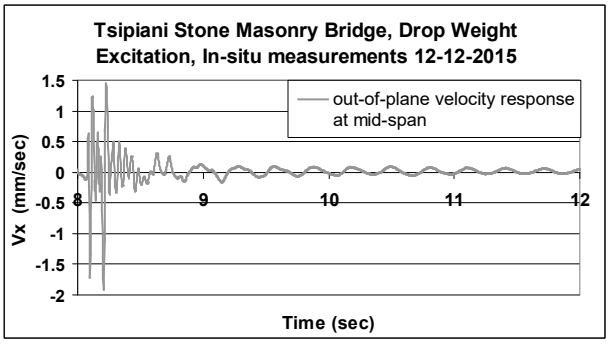

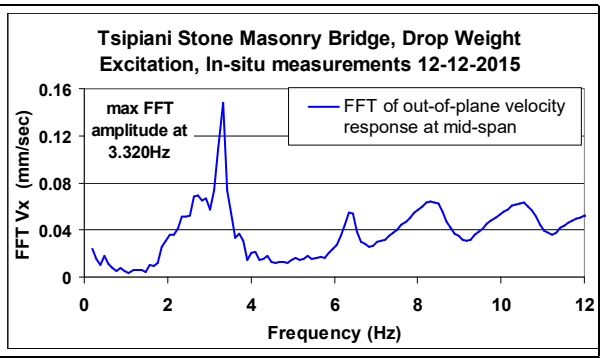

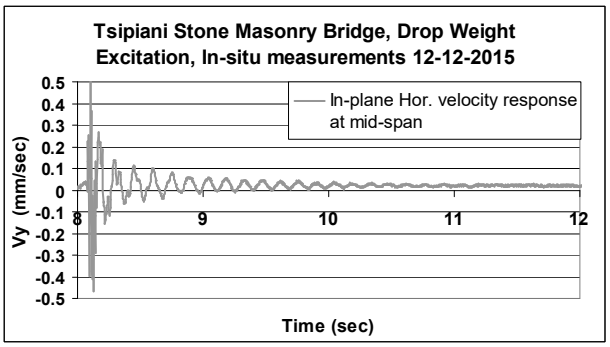

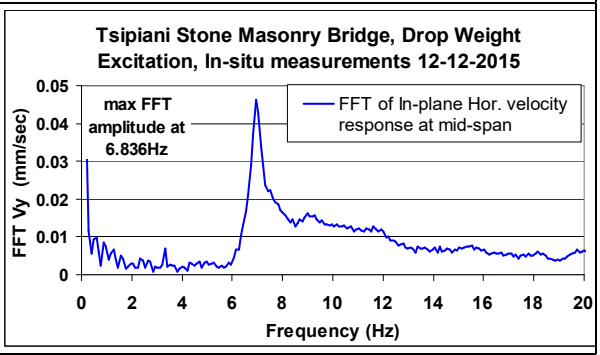

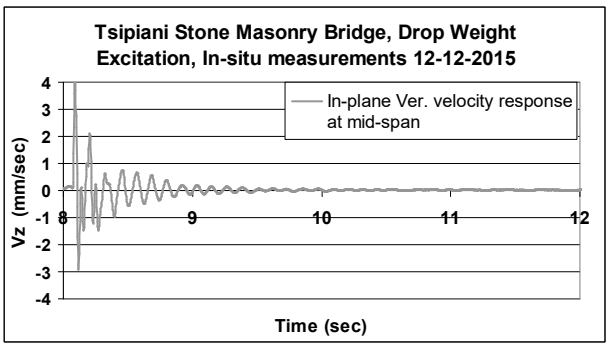

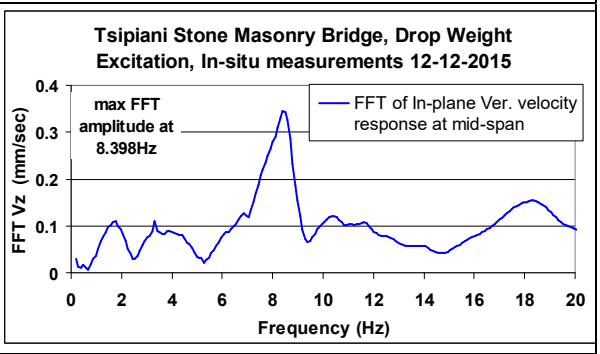

Figure 7a, 7c and 7e. Measured velocity response at mid-span of Tsipiani bridge

Figure 7b, 7d and 7f. FFT plots of the measured velocity response at mid-span of Tsipiani bridge

Measurements from drop weight excitation were repeated many times. Moreover, the velocity response was measured at by placing the sensors at three locations, as shown in figure 3 (left sensor, mid sensor, right sensor). Figures 7a to 7f represent the response at the mid-span of the main central arch of the Tsipiani bridge as recorded by mid-sensor during a drop weight test with the code name MIDLJ016, denoting that the drop weight was applied also at the mid-span location of this bridge. During subsequent tests the drop weight was also applied at locations near either the left sensor or the right sensor. From all these tests an effort was made to deduce the most significant eigen-modes and eigen frequencies for this structure,

which are listed in table 1. In the 1st row of this table 1 the values of the eigen-frequencies of the main in-plane eigen-modes are listed whereas the eigen-frequencies of the main out-of-plane eigen-modes are listed in the 2nd row of this table.

Table 1. Measured eigen-frequencies for four stone masonry bridges

Measured eigen-frequencies (Hz) for the ***Tsipiani Bridge.***			
In-Plane	1st Asymmetric 6.934Hz	2nd Symmetric 8.549Hz	3rd Symmetric 14.209Hz
Out-of Plane	1st Symmetric 3.320Hz	2nd Asymmetric 6.348Hz	3rd Symmetric 12.207Hz

As can be seen, the drop weight excitation could produce at the dominant frequencies vibrations at least one order of magnitude larger than the wind excitation. From these measurements an attempt was also made to obtain an estimate of the damping ratio for the dominant in-plane and out-of-plane frequencies. As is depicted in figure 5, the 1st symmetric out-of-plane vibration (x-x) that is excited by the wind has an eigen-frequency value equal to 3.369Hz whereas, as depicted in figures 7a and 7b for the drop weight excitation, the eigen-frequency value for this 1st symmetric out-of-plane mode is equal to 3.320Hz. An estimate of the damping ratio value equal to 1.5% was found for this 1st symmetric out-of-plane (x-x) eigen-mode, obtained from the measured mid-span out-of-plane response for Tsipiani bridge (see figure 8).

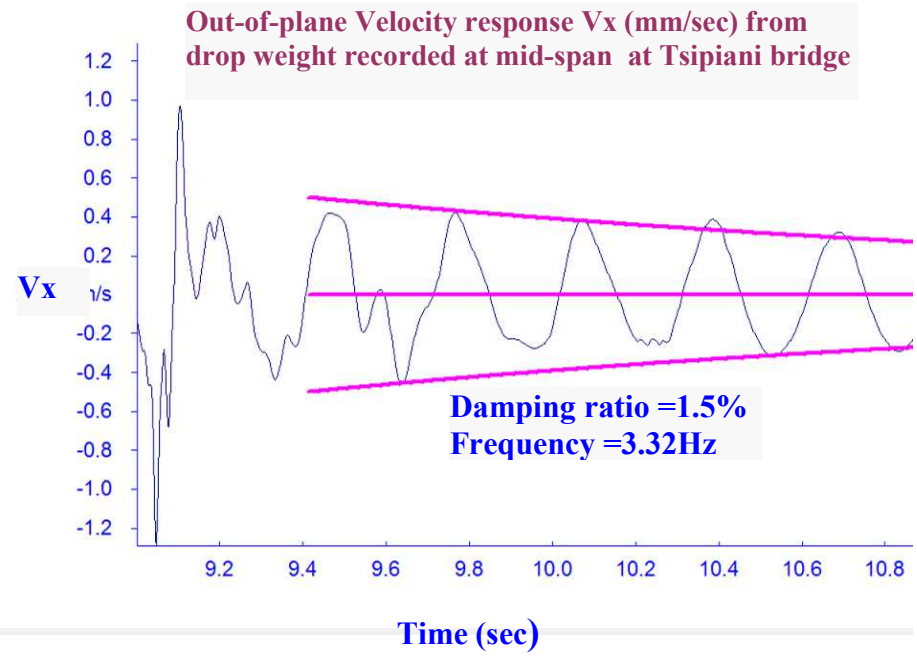

Figure 8. Estimate of damping ratio for the 1st symmetric out-of-plane eigen-mode.

Similarly, an estimate of the damping ratio value equal to 4.6% was found for the 2nd non-symmetric in-plane eigen-mode, obtained from the measured mid-span in-plane (z-z) response for Tsipiani bridge (see figure 9). It is interesting to see that the damping ratio for the 1st out-of-plane symmetric eigen-mode is noticeably smaller than the corresponding value for the 2nd symmetric in-plane eigen-mode. The eigen-mode shapes and eigen-frequencies that

were deduced from all the in-situ measurements for the Tsipani stone masonry bridge are depicted in figure 10.

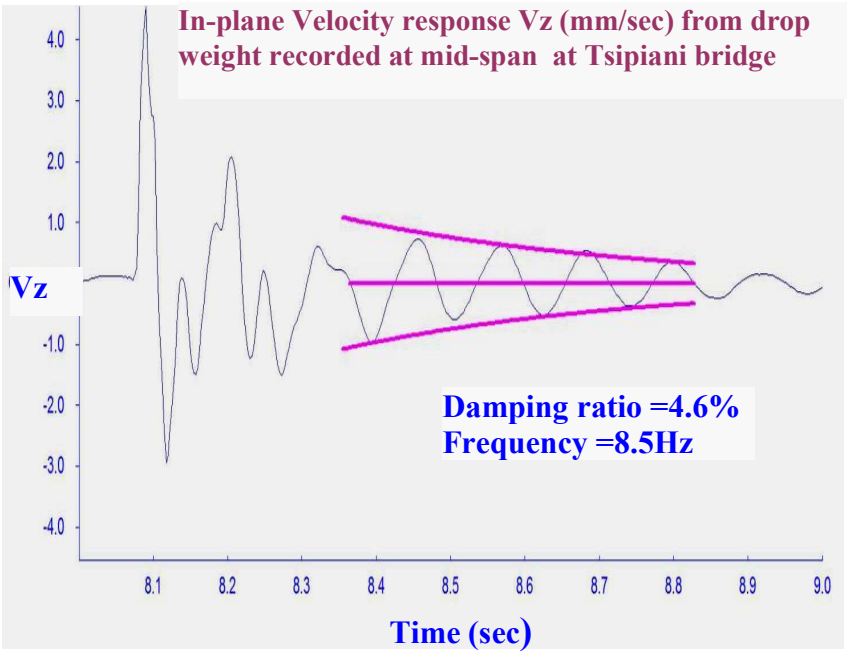

Figure 9. Estimate of damping ratio for the 2nd symmetric in-plane eigen-mode.

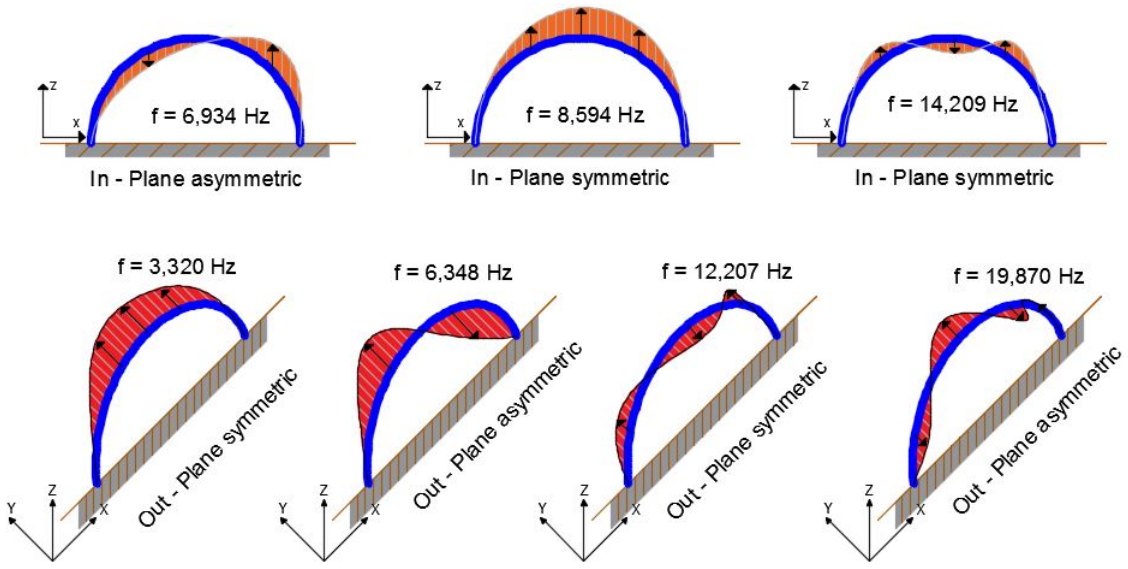

Figure 10. Eigen-modes and eigen-frequencies for Tsipiani stone masonry bridge deduced from all the in-situ measurements.

3 NUMERICAL SIMULATION OF THE VIBRATORY EIGEN-MODES FOR TSIPIANI BRIDGE

In this section the eigen-frequencies and eigen-modes of Tsipiani stone masonry bridge will be predicted through a numerical simulation process. Initially, this numerical simulation will be based on elastic behaviour, assuming the stone masonry as an orthotropic continuous medium and limiting the numerical model at approximately the interface between the end abutments and the rocky river banks thus introducing boundaries at these locations [10]. For simplicity purposes, the bulk of these numerical simulations is made in the 3-D domain representing the bridge structure with its mid-surface employing thick shell finite elements [11]. The various main parts of this stone masonry bridge, that is the primary and the secondary arches, the abutments, the deck, the mandrel walls and the parapets were simulated in such a way that narrow contact surfaces could be introduced between them, representing in this way a different "softer" medium. All available information, measured during the in-situ campaign, on the geometry of each one of these parts was used in building up these numerical simulations. The mechanical property values obtained from the stone and mortar sample tests were utilized (see Manos et al. (2016) [1]). Moreover, there is important information that is needed in order to form with some realism the boundary conditions at the river bed and banks [11]. The lack of specific studies towards clarifying in a systematic way all these uncertainties represents a serious limitation in the numerical simulation process.

The approximation adopted in this study is a process of back simulation [6], [7]. That is, adopting values for these unknown mechanical stone masonry properties, respecting at the same time all the measured geometric details, that result in reasonably good agreement between the measured and predicted in this way eigen-frequency values. Following this approximate process two distinct cases of boundary conditions were introduced. In one series of numerical simulations all the boundaries, either at the river bed or the river banks, were considered as being fixed in these 3-D numerical simulations. This is denoted in the predicted eigen-frequency values in figures 11a to 11h where this is denoted as fixed boundary conditions. Alternatively, the rotational degrees of freedom were released all along the locations where the abutments are supported at the river banks thus excluding the footings. This is denoted in the predicted eigen-frequency values in figures 12a to 12h as pinned boundary conditions. It was observed from this sensitivity analysis that was performed by Manos et al. (2016) for a number of stone masonry bridges that this variation in the boundary conditions approximation influences, as expected, the out-of-plane and not the in-plane stiffness of the studied stone masonry bridges. Moreover, for the Tsipianis Bridge whereby the main central arch is supported at the North end in adjacent arches rather than in a rocky river bank this influence of the variation of the boundary conditions, as expected, is again less pronounced. The value of the corresponding measured eigen-frequency values is also presented in figures 11a to 11h and 12a to 12h within brackets in blue bold print next to the numerically predicted value. As can be seen from this comparison, through this back analysis procedure reasonably good agreement is reached between the numerically predicted eigen-frequency values with the ones deduced from the in-situ measurements. Moreover, from this comparison it can also be seen that the fixed boundaries yield better agreement between predicted and measured eigen-frequency values for the out-of-plane response eigen-modes than when pinned boundaries are employed. As already commented, the change in boundary conditions does not influence the in-plane response eigen-mode predicted values.

Old masonry bridge of Tsipiani: Fixed boundary conditions

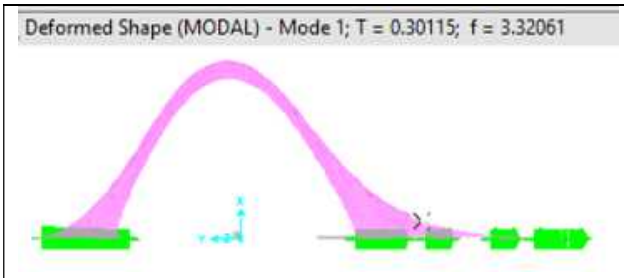

a) 1st out-of-plane symmetric f=3.32Hz (**3.32Hz**)

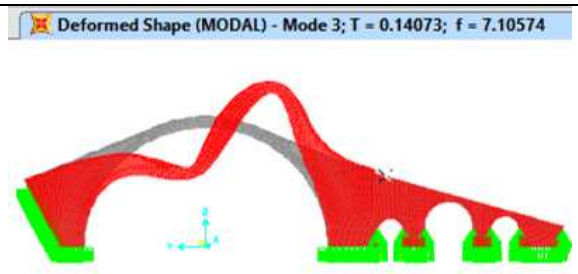

b) 1st in-plane asymmetric f=7.106Hz (**6.93Hz**)

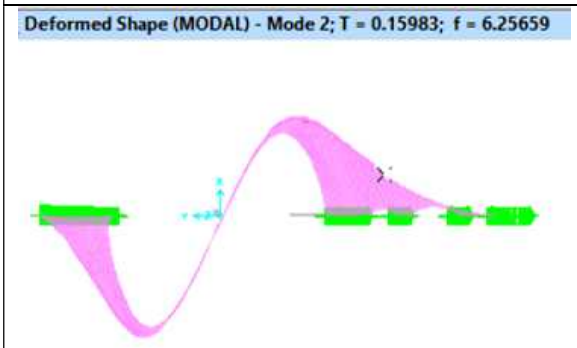

c)2nd out-of-plane asymmetric f=6.26Hz (**6.35Hz**)

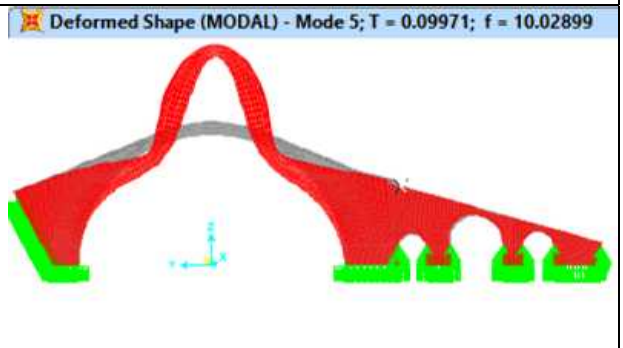

d) 2nd in-plane symmetric f=10.03Hz (**8.59Hz**)

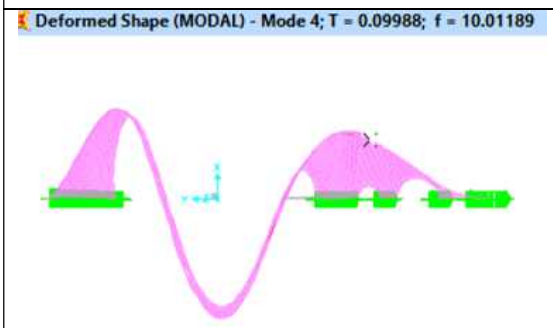

e) 3rd out-of-plane symmetric f=10.01Hz (**12.21Hz**)

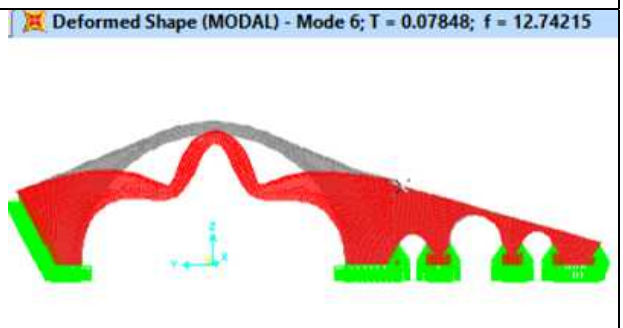

f) 3rd in-plane symmetric f=12.74Hz (**14.21Hz**)

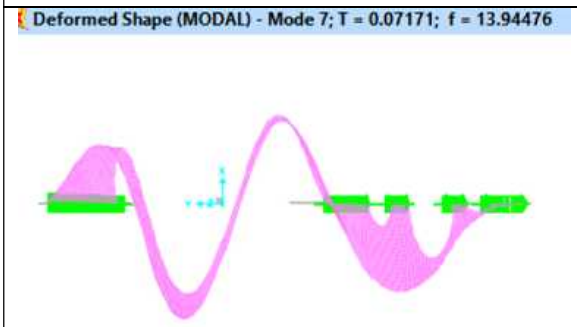

g) 4th out-of-plane asymmetric f=13.95Hz (**19.87Hz**)

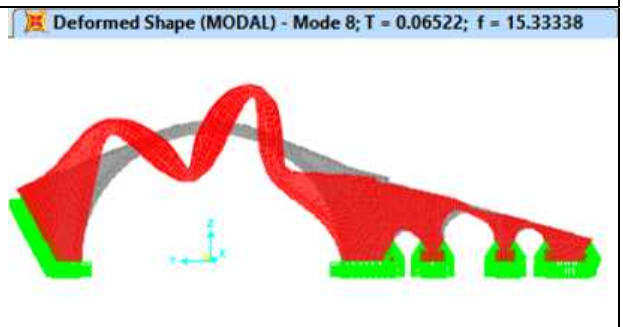

h) 4th in-plane asymmetric f=15.333Hz

Figures 11a, c, e, g. Out-of-plane eigen-modes for **fixed boundaries**. Tsipiani stone masonry bridge

Figures 11b, d, f, h. In-plane eigen-modes for **fixed boundaries**. Tsipiani stone masonry bridge

Old masonry bridge of Tsipiani: Pinned boundary conditions

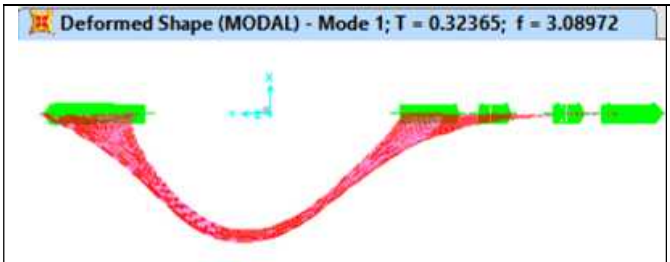

a) 1st out-of-plane symmetric f=3.09Hz (**3.32Hz**)

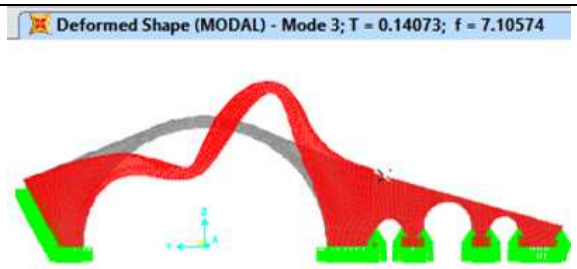

b) 1st in-plane asymmetric f=7.106Hz (**6.93Hz**)

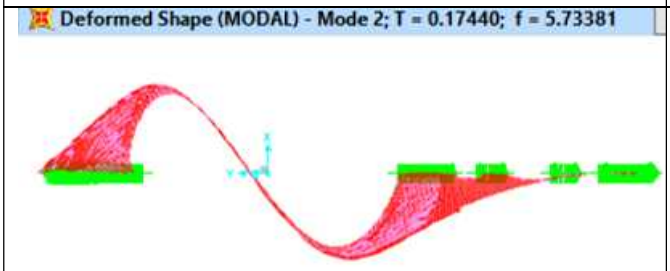

c)2nd out-of-plane asymmetric f=5.73Hz (**6.35Hz**)

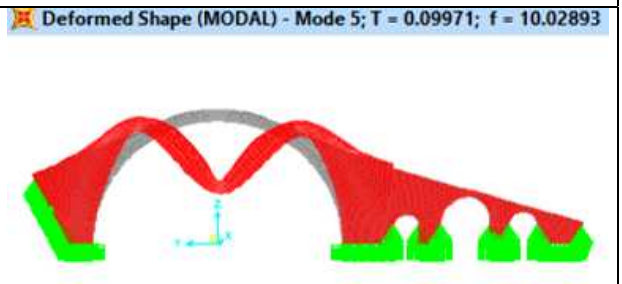

d) 2nd in-plane symmetric f=10.03Hz (**8.59Hz**)

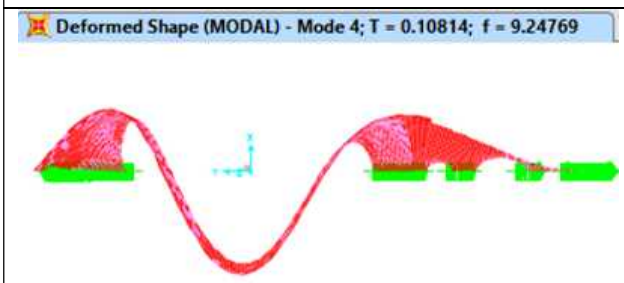

e) 3rd out-of-plane symmetric f=9.25Hz (**12.21Hz**)

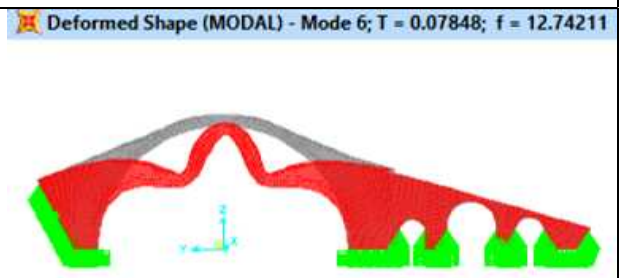

f) 3rd in-plane symmetric f=12.74Hz (**14.21Hz**)

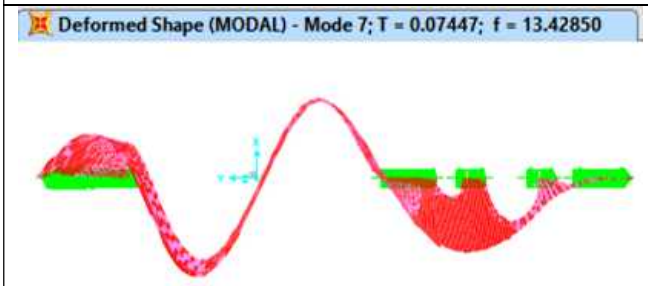

g) 4th out-of-plane asymmetric f=13.43Hz (**19.87Hz**)

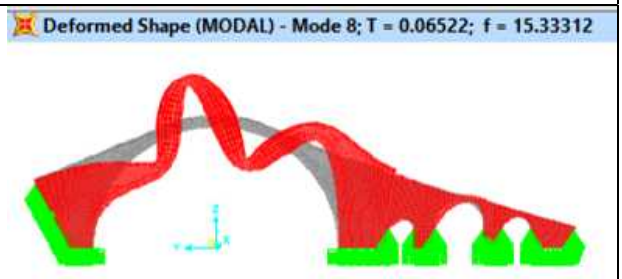

h) 4th in-plane asymmetric f=15.333Hz

Figures 12a, c, e, g. Out-of-plane eigen-modes for **pinned boundaries**. Tsipiani stone masonry bridge

Figures 12b, d, f, h. In-plane eigen-modes for **pinned-boundaries**. Tsipiani stone masonry bridge

4 SIMPLIFIED NUMERICAL SIMULATION OF THE SEISMIC BEHAVIOUR OF THE PLAKA BRIDGE.

This section includes results of a series of numerical simulations of the Plaka bridge when it is subjected to a combination of actions that include the dead weight (D) combined with accidental forces. This bridge replaced an older bridge at the same place that collapsed from flooding of Aracthos river in 1860. The first attempt in rebuilding this collapsed bridge also collapsed in 1863 during the opening day. The Plaka bridge depicted in figure 13, one of the most spectacular stone masonry bridges was built in 1866 by the chief mason Kostas Mpekas and survived till January 2015 despite the structural damage that suffered during the World War II. It collapsed on the 2nd of February 2015 again from flooding of Arachtos river (figures 14 and 15). The span of the main central arch was equal to 40m rising at a height of 20m. The total length of this bridge was over 60m and the width of the deck at mid-span of the central arch 3.20m As can be seen in figure 13, a secondary arch is constructed at the right side of the main arch resulting in a mid-pier that is founded on the river bed. Moreover, a large arch-shape opening is present at the left abutment with its foundation being also partly supported on the river bed. The presence of these two openings (right secondary arch and the left relief) was not sufficient to protect the structure from the forces caused by this recent flooding.

Figure 13. The Plaka stone masonry bridge prior to its collapse on 2nd February 2015.

.Because almost all the stone masonry bridges in Greece have been built mostly for relatively light live load levels resulting from the crossing of pedestrians or animal flocks their structural vulnerability due to traffic conditions is not an issue. Instead, seismic forces or flooding of the narrow gorge currents that these bridges cross are causes of structural damage that may lead to collapse, as demonstrated from the Plaka bridge (see figures 14a, 14b, 15a, and 15b). Apart from the hydro-dynamic loads that a stone masonry bridge is subjected to from a flooded current, one of the main sources of distress that may lead to partial or total collapse is the deformability of the foundation. This seems to be the case for the mid-right pier of Plaka bridge as depicted in figure 15b. The present investigation is three-fold. Initially, with a first numerical simulation attempt the dynamic characteristics of this bridge will be studied in terms of eigen modes and eigen-frequencies, as was done for the Tsipiani brisge. Unfortunately, no direct comparison between predicted and measured values can be performed this time due to the collapse of the Plaka bridge. However, the same assumptions that were fol-

lowed before in the numerical simulation of the Tsipiani bridge as well as of a number of other stone masonry bridges (see Manos et al. (2016) [1], will also be adopted here. Consequently, it is believed that this will provide sufficient validity to this type of numerical simulation because of the good agreement between measurements and predictions that was achieved in all the other cases that were numerically simulated in this way.

Figure 14a. Flooding of river Arachtos on 2nd February 2015

Figure 14b. The collapsed Plaka bridge during the visit of December 2015.

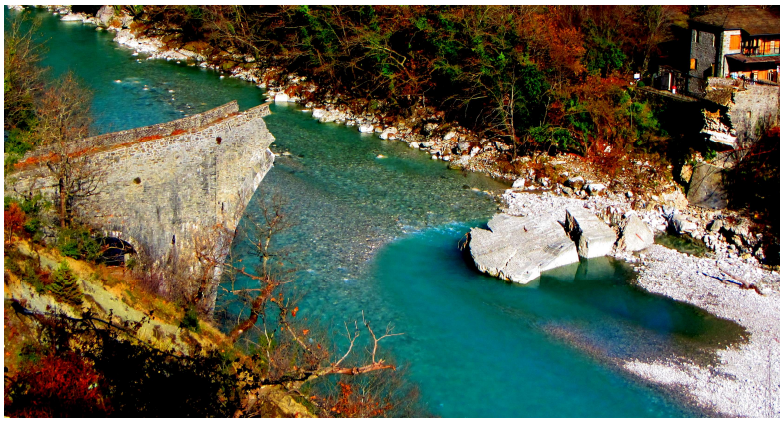

Figure 15a. View of the Plaka bridge after the collapse from the West bank. Note the total destruction of the mid-pier (see also figure 7d). December 2015.

Figure 15b. Close up of the total destruction of the mid-pier of Plaka bridge (see also figure 7d).

Next, through a simplified numerical simulation the flooding and the structural damage from the 1944 explosion are studied by numerically simulating the state of stress of the bridge for these loading conditions. Finally, an additional numerical simulation will try to study the state of stress in the case that this bridge, before its collapse, was subjected to a design earthquake

4.1 Dynamic characteristics of the Plaka stone masonry bridge.

The same type of numerical simulation that was described in section 3 will also be followed here. More information on the material properties are given by Manos et al. (2016) [1]. Two distinct cases of boundary conditions for the abutments were also studied here as was done for the Tsipiani bridge, namely fixed and pinned boundary conditions. The obtained numerical predictions of the eigen-modes and eigen frequencies for the Plaka bridge are depicted in figure 16 for both cases of boundary conditions. Due to the size of this bridge as well as because of the presence of the left and right secondary arches the 1st symmetric out-of-plane eigen-

mode has relatively low eigen-frequency values equal to 2.068Hz and 1.896Hz, for the fixed and pinned boundaries, respectively. This is also true for the higher order out-of-plane eigen modes. This is a clear indication of the flexibility of this bridge, mainly in the out-of-plane direction which is also the direction of loading during river flooding as well as from the horizontal component of an earthquake excitation in a direction perpendicular to the longitudinal (y-y) axis of this bridge.

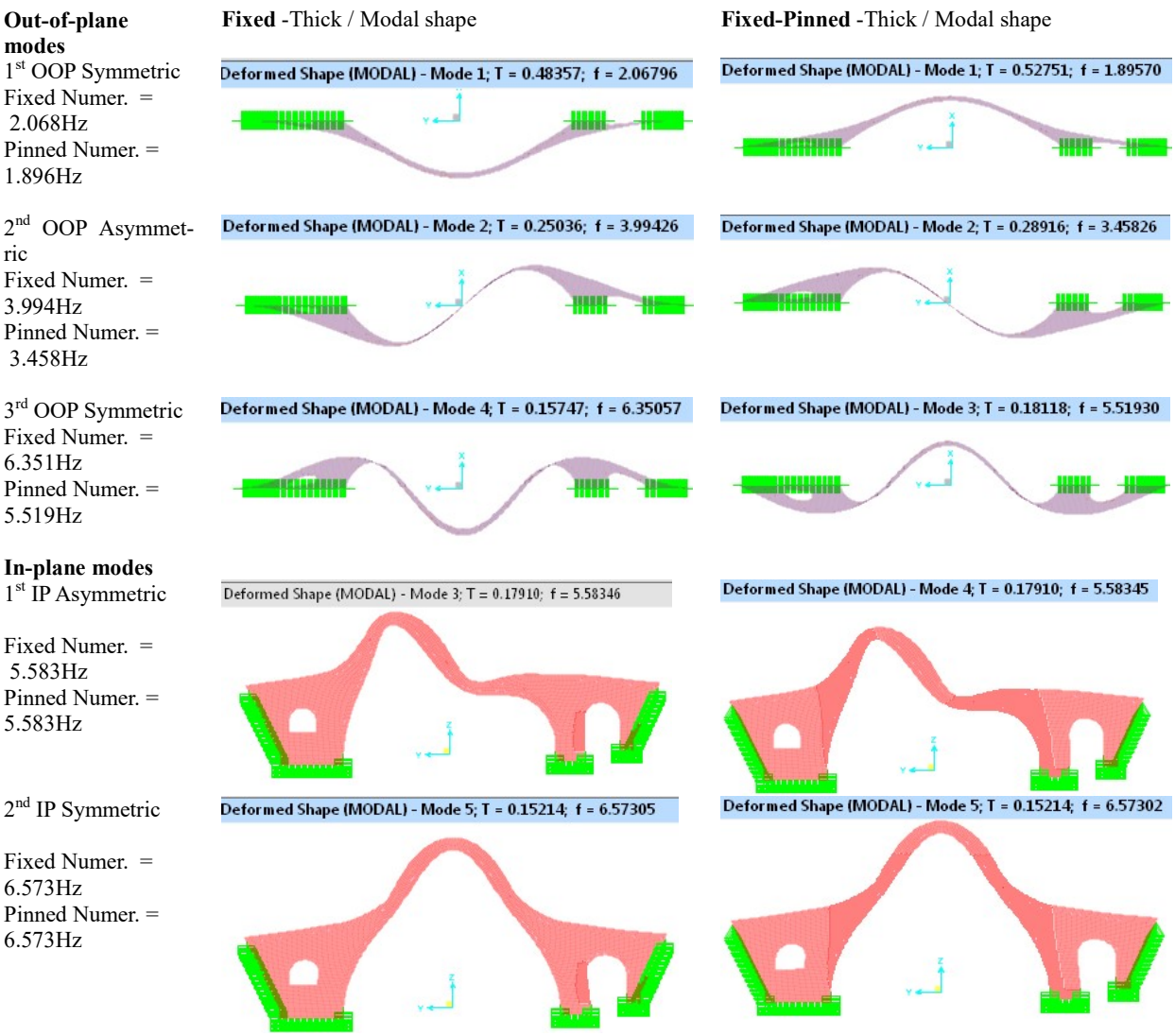

Figure 16. Numerical eigen-frequency values and thencorresponding eigen-modes for the Plaka Bridge.

4.2 Simplified numerical simulation of the Plaka stone masonry bridge for flooding conditions.

In this section the results of a simplified numerical simulation of the Plaka bridge under flooding conditions are presented. Towards this objective the numerical simulation discussed in the previous section 4.1. is utilized on the assumption that it constitutes a realistic numerical approximation. The behaviour of the Plaka bridge is examined for two loading conditions. The first loading condition is that of the gravity forces.

The second loading condition is the one that combines the gravity forces with the simplified flooding loads. In the present study, due to lack of data that can ascertain the velocity of the flow of the river at the bridge and the maximum level of the water during the 2nd of February flooding no attempt was made to estimate the distribution of the hydrodynamic pressures on these parts of the Plaka bridge that was submerged in the flooded river (see figure 14a). As can be seen also in figure 17 the flow of the river, even after the collapse of the Plaka bridge, is quite turbulent and flows on top of the left opening. In contrast, we can observed how this turbulent flow have subsided the week following the collapse, with the remains of the mid-pier in the for-ground of figure 18.

Figure 17. Collapse of Plaka bridge from the 2nd of February, 2015 flooding

Figure 18. Collapse of Plaka bridge from the 2nd of February, 2015 flooding

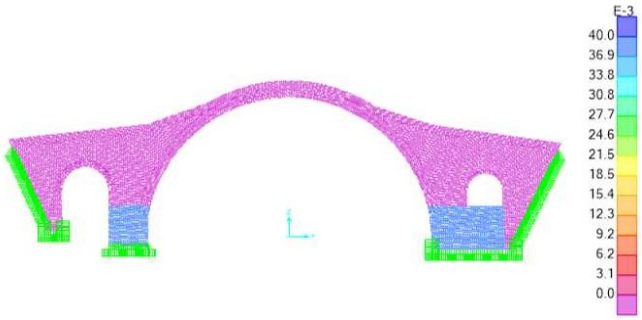

Figure 19. Simplified distribution of the hydrodynamic loads.

Figure 19 depicts with blue colour the simplified representation of the flooding load adopted in the present study as being applied in the lower part of the middle pier and the right abutment. This load was applied as a uniformly distributed pressure acting in these parts of the bridge from the level of the river-bed to foundation of the mid-pier interface till the low rim of the right opening. The amplitude of this pressure was equal to 0.04MPa. deduced from maximum velocity of the flow deduced from an assumed height differential that generated this flooding event. These flooding forces were assumed to be static in nature ignoring any dynamic fluid-structure interaction. In light of the nature of these assumptions it can be argued that the used static load to approximate the hydrodynamic forces underestimates the actual effect that the severe 2nd of February flooding had on the Plaka bridge. This investigation, apart from considering in the described simplified way the hydrodynamic loads on the Plaka bridge, attempted to also study the deformability of the foundation of the mid-pier, which is believed to be of significance [26].

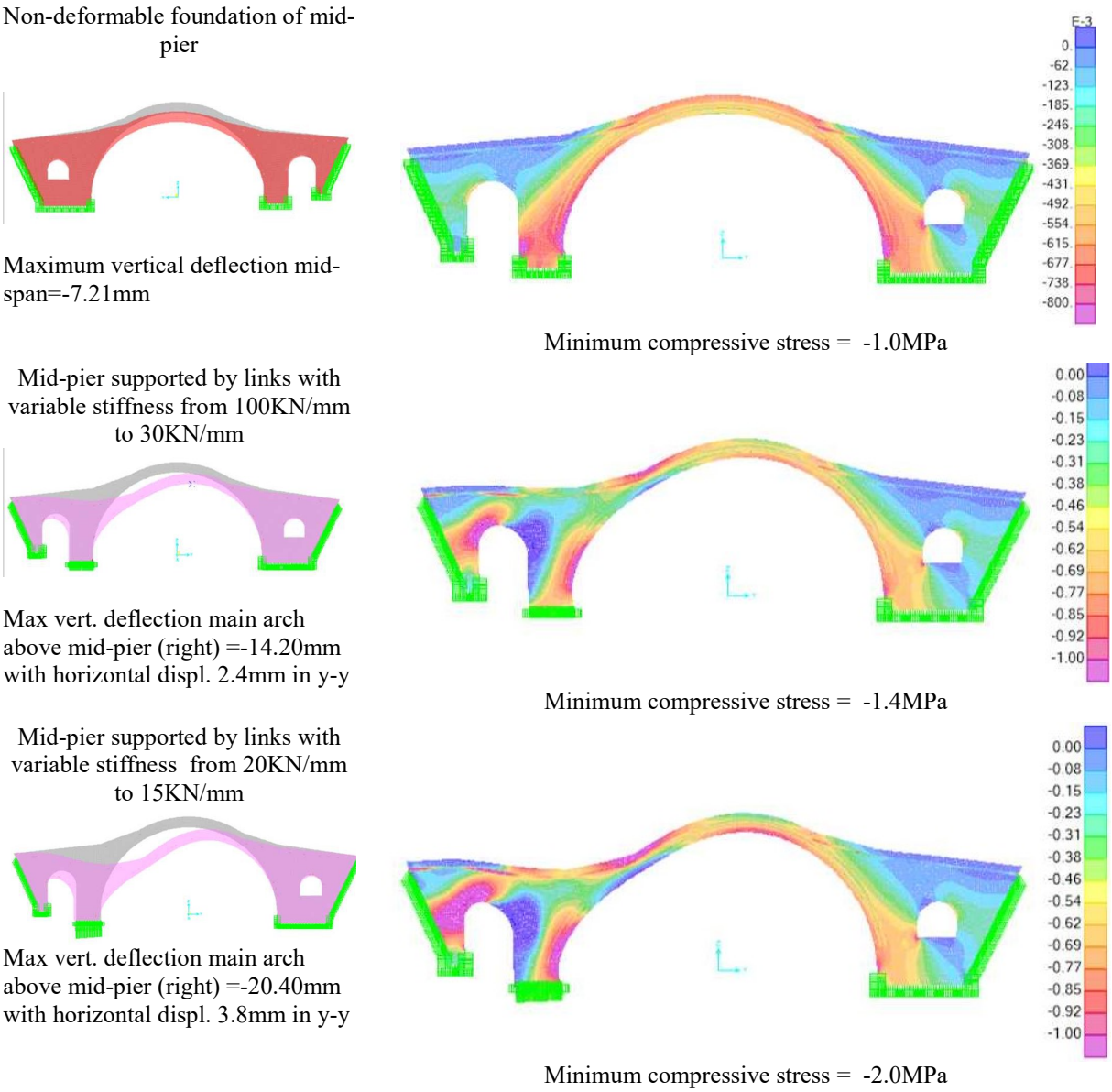

Figure 20. Variation of minimum compressive stresses with the deformability of the mid-pier. Only Gravity Forces

The support condition of the mid-pier foundation, which as already described lies in the river bed, could also be influenced from erosion due to the river flow in the long term as well as in the short term during the strong and turbulent flow prior to the collapse of 2nd February 2015. In order to examine this parameter in the framework of the current simplified numerical investigation the following approach was used. Three different stiffness conditions were examined in order to simulate the deformability of the mid-pier foundation. This was achieved employing 3-D linear springs to connect in the vertical direction the lower level of the mid-pier foundation with underlying medium, which was assumed to be non-deformable. The stiffness of these springs in the horizontal direction was assumed to be infinite. In the first case these spring were assigned with a very large axial stiffness value in the vertical direction, thus representing a non-deformable mid-pier foundation. In the second case these springs were provided with a stiffness value in the vertical direction varying from 100KN/mm at the left end corner of this mid-pier foundation to a relatively low value (30KN/mm) at the right end corner, which is located further inwards in the river. Finally, in the third case the flexibility of the mid-pier foundation was increased even further assigning axial stiffness values in

the vertical direction equal to 40KN/mm for the left end corner spring and equal to 7KN/mm for the right end corner spring. For the springs lying in between their axial stiffness in the vertical direction was set equal to values varying linearly with distance between the previously mentioned values.

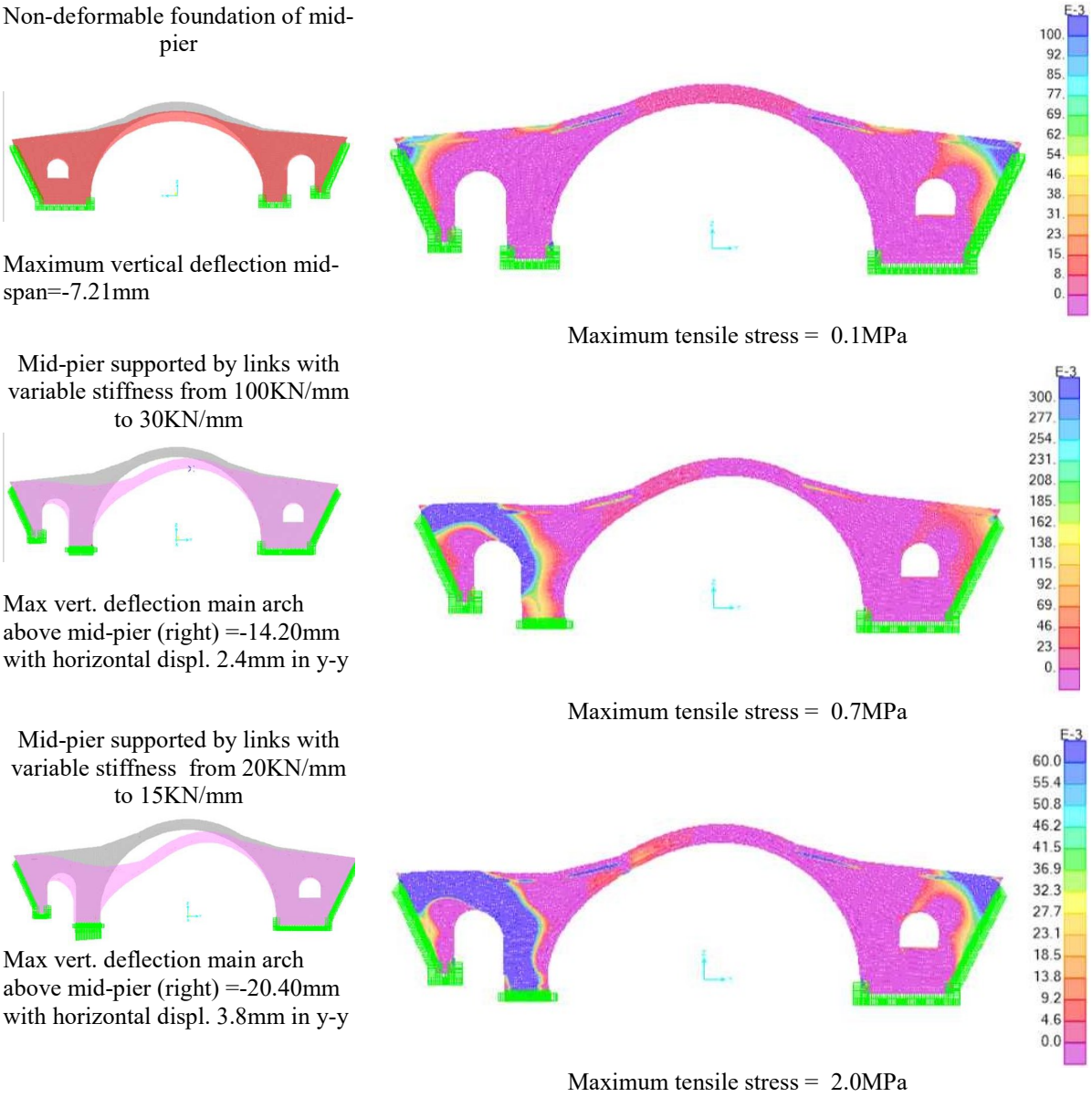

Figure 21. Variation of maximum tensile stresses with the deformability of the mid-pier. Only Gravity Forces

Figures 20 and 21 show the deformation patterns of the Plaka bridge together with either the minimum compressive or the maximum tensile stresses, respectively. This is done when the structure is subjected to gravity forces. In figures 22 and 23, this is done when the gravity forces are applied together with the simplified flooding loads, as described before. In all these figures the deformation patterns and the stress distribution plots are given in each figure for the three specific cases of the mid-pier foundation flexibility, as explained before; that is a) for non-deformable foundation, b) for a relatively stiff foundation and finally c) for a relatively flexible foundation. In cases b) and c) the flexibility of the foundation is introduced in a variable fashion along the foundation width in a way that attempts to numerically simulate long and short term erosion of the foundation at this location.

Non-deformable foundation of mid-pier

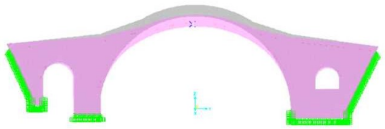

Maximum vertical deflection mid-span=-7.35mm with horizontal displ. 0.95mm in x-x (river flow)

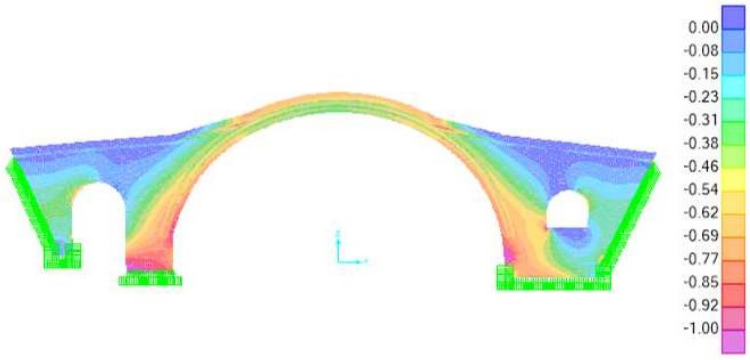

Minimum compressive stress = -1.1MPa

Mid-pier supported by links with variable stiffness from 100KN/mm to 30KN/mm

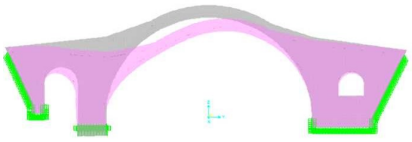

Max vert. deflection main arch above mid-pier (right) =-14.10mm with horizontal displ. 2.8mm in y-y, and 0.87mm hor. displ. (out-of-plane, x-x direction, flow of river)

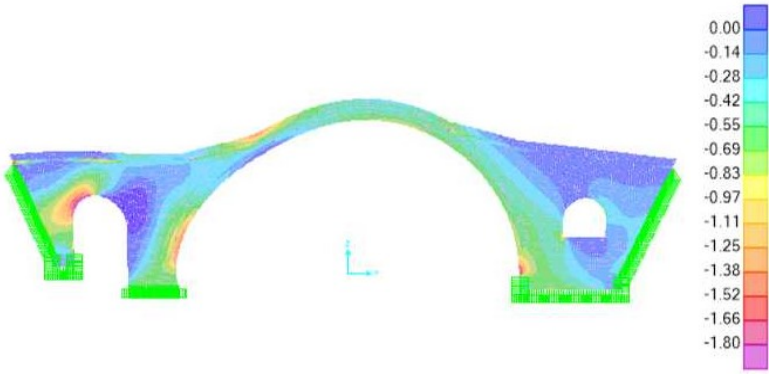

Minimum compressive stress = -1.8MPa

Mid-pier supported by links with variable stiffness from 40KN/mm to 7KN/mm

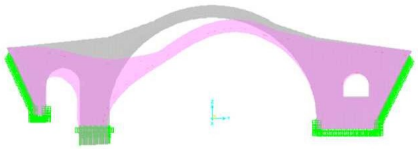

Max vert. deflection main arch above mid-pier (right) =-19.40mm with horizontal displ. 3.6mm in y-y, and 0.85mm hor. displ. (out-of-plane, x-x direction, flow of river)

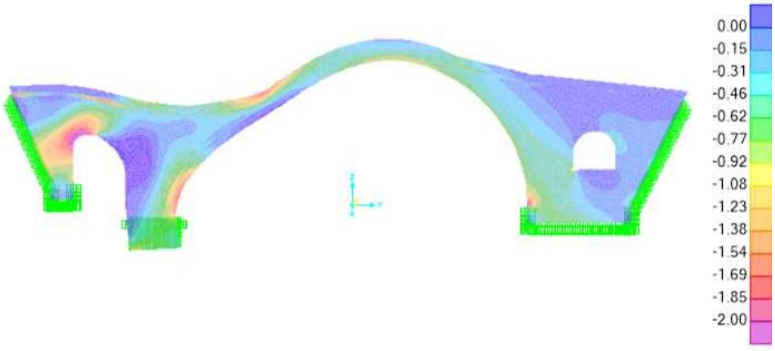

Minimum compressive stress = -2.2MPa

Figure 22. Variation of maximum compressive stresses with the deformability of the mid-pier. Gravity Forces together with hydrodynamic loads.

The obtained Plaka bridge deformation and stress (tensile as well as compressive) response in figures 21, 22 and 23, where the variation of the mid-pier foundation flexibility was introduced together with the simplified flooding loads, can be studied in a comparative way. Through the plotted peak deformation and stress values it can be observed that the flexibility of the foundation results in more detrimental response for the Plaka bridge than the applied flooding loadings. This is apparent from the larger values in terms of deformations and tensile stresses, where the mid-pier joins the main arch and the secondary right arch, due to the flexibility of the foundation rather that from the application of the flooding loads. This could be attributed to the simplified way in terms of amplitude, distribution and frequency content that the flooding loads were applied to the Plaka bridge. The peak tensile stress takes a value equal to 0.1MPa (top right of figures 21,22 and 23) when its foundation is non-deformable. For the case of quite flexible foundation conditions the tensile stress field at either the left or right mid-pier regions results in peak values equal to 2.5MPa and 0.43MPa, respectively (bottom left of figure

23). These values are well beyond the tensile strength of stone masonry, thus signifying potential structural damage. The deformation peak value is 7.35mm (out-of-plane) against 19.4mm for the for the non-deformable and deformable foundation cases, respectively.

Non-deformable foundation of mid-pier

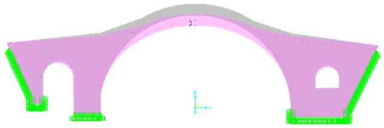

Maximum vertical deflection mid-span=-7.35mm with horizontal displ. 0.95mm in x-x (river flow)

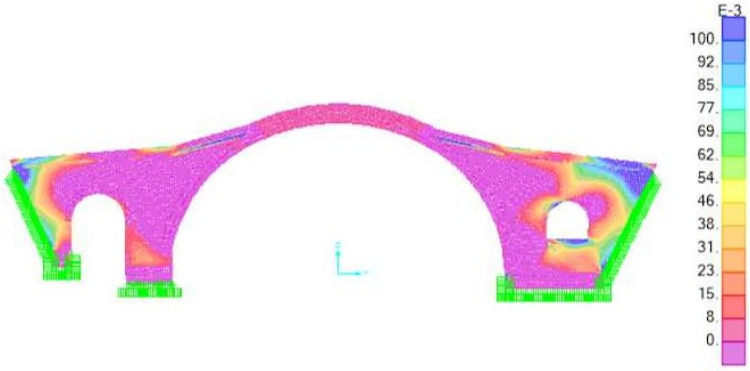

Maximum tensile stress = 0.1MPa

Mid-pier supported by links with variable stiffness from 100KN/mm to 30KN/mm

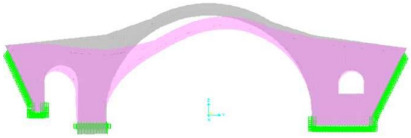

Max vert. deflection main arch above mid-pier (right) =-14.10mm with horizontal displ. 2.8mm in y-y, and 0.87mm hor. displ. (out-of-plane, x-x direction, flow of river)

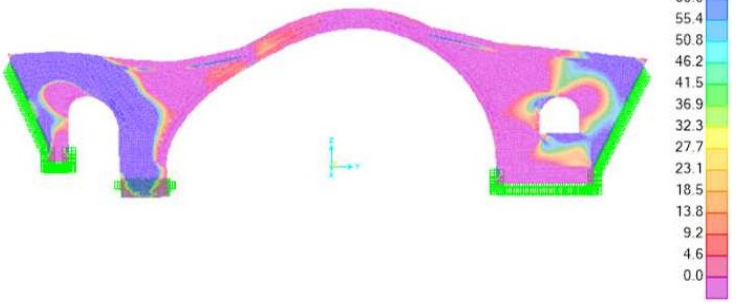

Maximum tensile stress = 1.0MPa

Mid-pier supported by links with variable stiffness from 40KN/mm to 7KN/mm

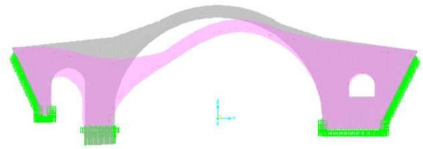

Max vert. deflection main arch above mid-pier (right) =-19.40mm with horizontal displ. 3.6mm in y-y, and 0.85mm hor. displ. (out-of-plane, x-x direction, flow of river)

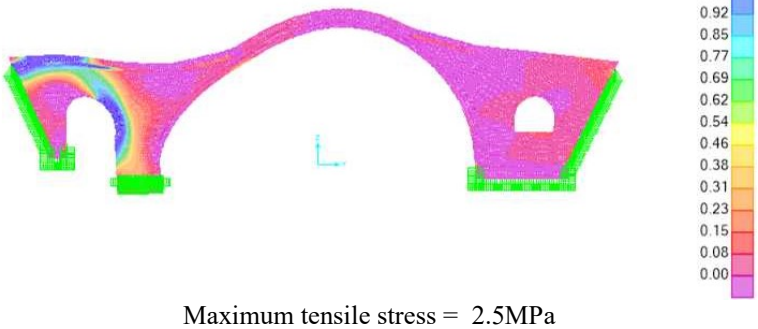

Maximum tensile stress = 2.5MPa

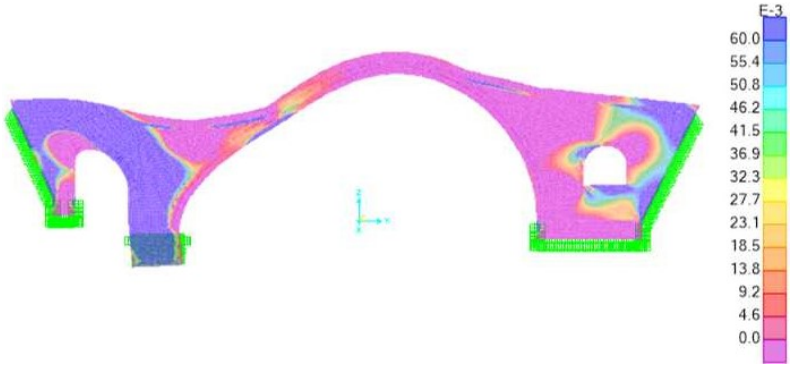

Maximum tensile stress = 0.43MPa at right side of main arch

Figure 23. Variation of maximum tensile stresses with the deformability of the mid-pier. Gravity Forces together with hydrodynamic loads.

4.3 Simplified numerical simulation of the damage that Plaka stone masonry bridge sustained from an explosion.

An additional part of this numerical study attempted to study the effect that the main arch of Plaka bridge sustained structural damage during an explosion that occurred in 1944, shown in some detail at the top of figure 24a. The numerical model of the bridge with the most flexible foundation conditions of the mid-pier was extended to simulate this structural damage at the region of the primary arch of the central main arch.

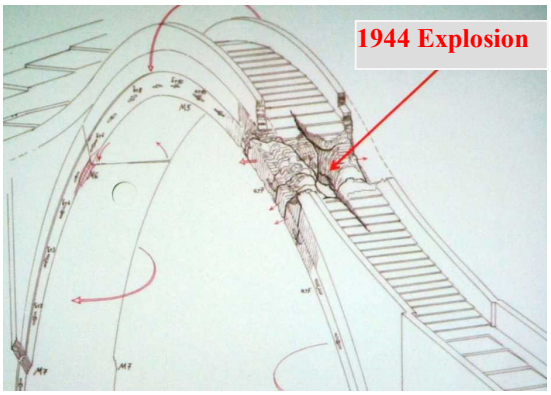

Mid-pier supported by links with variable stiffness from 40KN/mm to 7KN/mm
Damage part of big arch simulated with membrane and bending stiffness values 10% of the original values

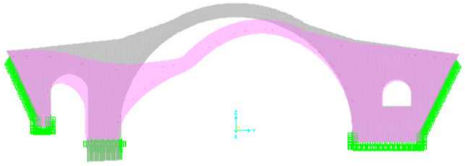

Max vert. deflection main arch above mid-pier (right) =-21.95mm with horizontal displ. 4.5mm in y-y, and 0.87mm hor. displ. (out-of-plane, x-x direction, flow of river)

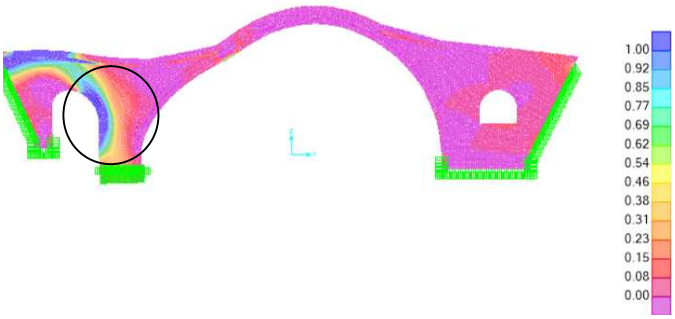

Maximum tensile stress = 2.579MPa at the left side of the mid-pier

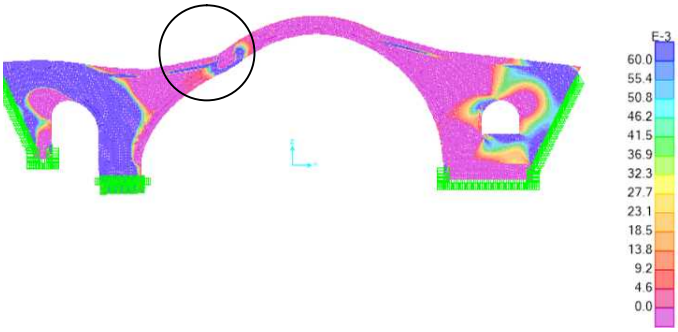

Maximum tensile stress = 0.764MPa at the damaged region located at the right side of main arch

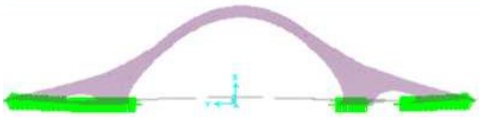

1st symmetric out-of-plane eigen-mode f=1.769Hz

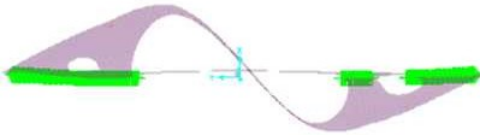

2nd asymmetric out-of-plane eigen-mode f=3.24Hz

1st asymmetric in-plane eigen-mode f=3.913Hz

Figure 24. Numerical simulation of the effect of the damage from the 1944 explosion

This was done by introducing to the damaged region of the primary central arch finite elements with bending and membrane stiffness values equal to 10% of the corresponding values used in the same model without the simulation of this damage. The obtained tensile stress peak response is depicted in the top right side of figure 24. By comparing the tensile response of figure 24 with that of figure 23, it can be concluded that this type of simulating the damage resulted in a 79% increase of the maximum tensile stress in a the region of the main arch that coincides with the damaged region (from 0.43MPa to 0.769MPa), located at the right side on the top of the mid-pier. It must be pointed out that some years after the explosion the damaged part was repaired with poured in place reinforced concrete. However, the effectiveness of this repair after a long period till the collapse of February 2105 is disputable. In the bottom of figure 24 the eigen-frequency values for the first two out-of-plane eigen-modes and the first in-plane eigen-mode are shown. By comparing these values with the corresponding values shown in figure 16 for the non-damaged structure with a non-deformable mid-pier foundation it can be seen that both the introduced damage and the mid-pier foundation flexibility reduces considerably the stiffness of the Plaka bridge both in the out-of-plane as well as in the in-plane direction. Whether this stiffness reduction coupled with the resulting values of the eigen-frequencies results in an amplification of the fluid-structure interaction for the 2nd of February 2015 flooding is a subject of further investigation.

4.4 Simplified numerical simulation of the Plaka stone masonry bridge for design earthquake conditions.

The seismic forces were defined by making use of the current definition of the seismic forces by EURO-Code 8 [12]. Towards this horizontal and vertical design spectral curves were derived based on the horizontal design ground acceleration. This value, as it is defined by the zoning map of the current Seismic Code of Greece, is equal to 0.24g (g the acceleration of gravity) for the location of the Plaka bridge [13], [14]. Furthermore, it is assumed that the soil conditions belong to category A because of the rocky site where this bridge is founded, that the importance and foundation coefficients have values equal to one (1.0), the damping ratio is considered equal to 5% and the behaviour factor is equal to 1.5 (unreinforced masonry). The design acceleration spectral curves obtained in this way are depicted in figures 26a and 25b for the horizontal and vertical direction, respectively. In these two figures (25a and 25b) the eigen-period range of the first twelve eigen-modes is also indicated (ranging between the low and the high modal period, see also figure 16). More details of the magnitude of the seismic forces generated at the Plaka bridge by these design response spectra are given by Manos et al (2016) [1].

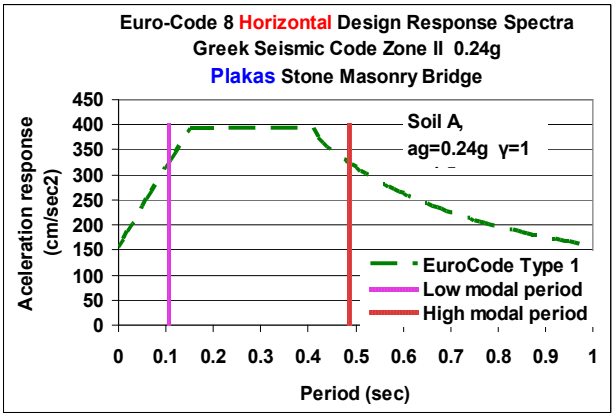

Figure 25a. Horizontal spectral curves for type-1 Euro-Code to be applied in Plaka Bridge.

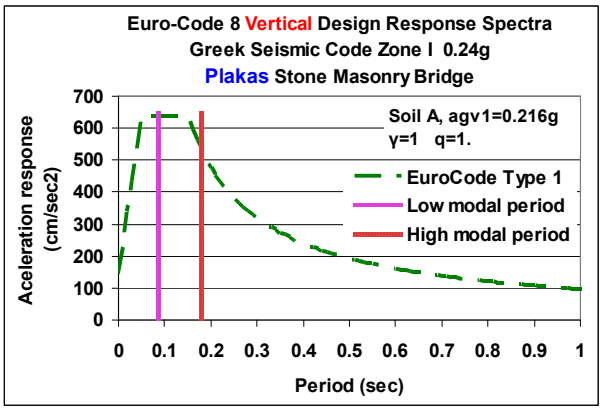

Figure 25b. Vertical spectral curves for type-1 Euro-Code to be applied in Plaka Bridge.

It must be pointed out that the flexibility of the foundation that was taken into account in the previous section was not considered here. Thus, the results to be presented and discussed in figures 26 and 27 were obtained for non-deformable mid-pier foundation. Moreover, the results were found from the combination of the gravity forces acting together with the seismic forces, as they resulted from the design spectra of figures 25a and 25b and a dynamic spectral analysis.

The deformed shape of the Plaka bridge for the design earthquake is shown in figure 26. As can be seen, the out-of-plane horizontal response attains large values at the crest of the main central arch. The peak value at mid-span (U1=51.87m) is 50 times larger than the corresponding value that was found when the bridge was subjected to gravity loads and flooding forces. The peak value at mid-span in the vertical direction (U3=23mm) is of similar amplitude to the one found when the bridge was subjected to gravity loads and flooding forces (see figures 22 and 23).

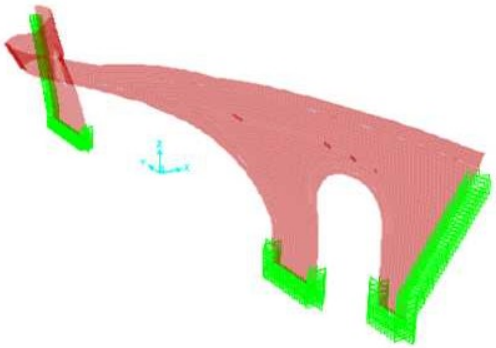

Fig. 26. Deformed shape of the Plaka bridge for the design earthquake. U1=-51.87mm (out-of-plane, hor. x-x), U2=3.4mm (in-plane hor. y-y), U3=-23.0 (in-plane ver. z-z).

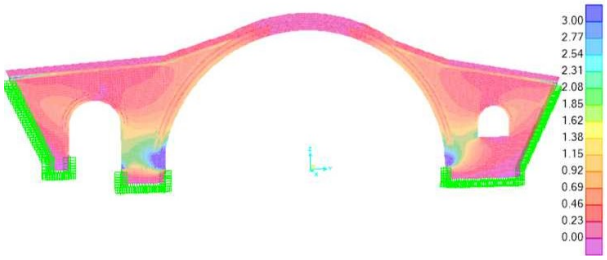

a) For loads Dead + EuroCode RS (u1+ u2 + u3) Comb 1. max S22 = 3.40MPa (Envelope Top face / Bottom face)

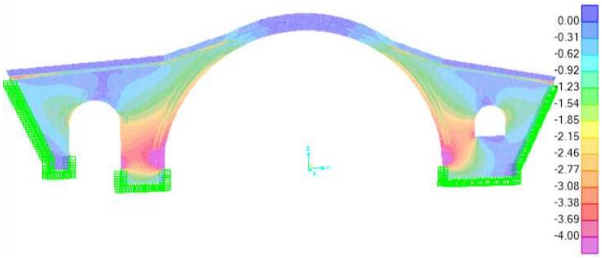

b) For loads Dead + EuroCode RS (u1+ u2 + u3) Comb 1. min S22 = -4.9MPa (Envelope Top face / Bottom face)

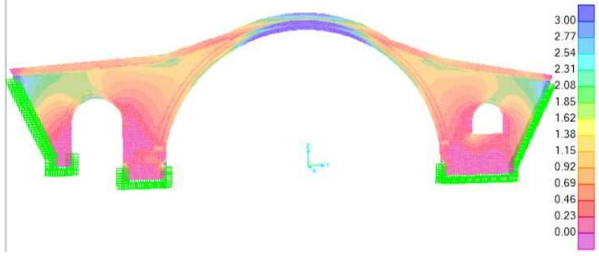

c) For loads Dead + EuroCode RS (u1+ u2 + u3) Comb 1. max S11= 5.73MPa (Envelope Top face / Bottom face)

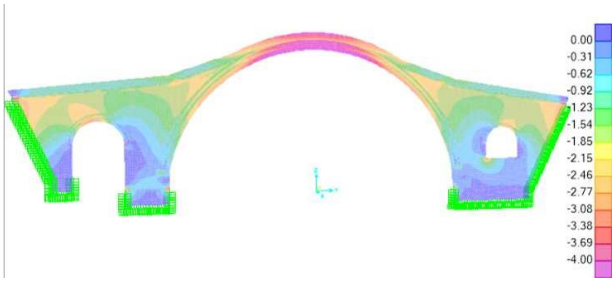

d) For loads Dead + EuroCode RS (u1+ u2 + u3) Comb1. min S11= -6.14MPa (Envelope Top face / Bottom face

Figure 27. State of stress through the distribution of stresses S11 and S22 for Plaka Bridge when subjected to gravity forces and seismic action.

The distribution of the maximum tensile and the minimum compressive stresses (S11 and S22) when the Plaka stone masonry bridge is subjected to gravity forces combined with the design earthquake, as defined before, are depicted in figures 27a to 27b. As can be seen from figures 27a and 27c the peak maximum tensile stress field develops at the crest of the main central arch (S11=5.73MPa) as well at the foot of the mid-pier (S22=3.40MPa, at the inner side). Similarly, the peak minimum compressive stress field develops again at the crest o the main central arch (S11=-6.14MPa) as well as at the foot of the mid-pier (S22=-4.9MPa).

These peak compressive values are well below the compressive strength of the stone masonry. On the contrary the peak tensile values are many times above the tensile strength of the stone masonry thus indicating the severe potential structural damage of the Plaka bridge from the design earthquake. The most vulnerable parts of the bridge, as obtained from the location of the peak tensile stress concentration, is a wide area at the crest of the main central arch of the bridge as well as the mid-pier internal side footing.

5 CONCLUSIONS

1. Stone masonry construction has a long tradition in many places worldwide. Stone masonry bridges built many centuries ago are one such example. Despite the rigidity and resilience of stone masonry bridges they are in need of maintenance in order to preserve them as part of the built cultural heritage. Towards this end in-situ measurement campaigns were conducted on a number of stone masonry bridges in order to identify their dynamic characteristics in terms of eigen-frequencies, eigen-modes and damping properties. This information is believed to represent a valuable basis for building realistic numerical simulations of the structural behaviour of such bridges as well as for their structural health monitoring.

2. The simplified numerical analyses yielded numerical predictions of bridge deformations and stresses that are useful in understanding the structural behaviour and the structural damage potential for such masonry structures. The structural performance of Plaka bridge that collapsed due to flooding in February 2015 was also studied. The structural behaviour of this bridge was examined when subjected to the gravitational forces combined with either simplified flooding loads or a design earthquake. Moreover, the structural damage that this bridge sustained during an explosion in 1944, was also examined together with the flooding loads.

3. As shown from the numerical predictions, the flexibility of the foundation, which may be partly attributed to long or short term erosion of the bridge footings, results in more detrimental response for the Plaka bridge than the applied simplified flooding loads. However, this may be due to the fact that the current investigation ignored any dynamic effects from fluid-structure interaction. The obtained numerical predictions from the numerical simulation of the structural damaged sustained by this bridge during the 1944 explosion leads to a dominant tensile stress field at the regions of the main and secondary arches on top of the mid-pier. These predicted peak tensile stress values are well beyond the stone masonry strength. Consequently, they could well have contributed towards the 2nd of February 2015 collapse.

4. The peak tensile values predicted when design seismic forces were applied for the Plaka bridge are many times above the tensile strength of the stone masonry thus indicating the severe potential structural damage for this old stone masonry bridge from the design earthquake. The most vulnerable parts of the bridge, as obtained from the location of the peak tensile stress concentration, is a wide area at the crest of the main central arch of the bridge as well as the mid-pier internal side footing. Thus, these earthquake vulnerability predictions for the Plaka bridge indicate that had the bridge not collapsed from flooding the design earthquake would have led to its structural damage and its partial collapse.

5. The integrity of the stone masonry in various parts of the bridge is an additional maintenance issue of considerable importance. Intervention recommendations for such bridge or attempts to rebuilt, as is the case for the Plaka bridge, should include clauses for applying preparatory actions of measurements and analyses like the ones included here together with es-

tablished principles that govern a major retrofitting / maintenance effort for cultural heritage together with effective retrofitting / maintenance techniques that are proven to be durable.

ACKNOWLEDGEMENTS

The assistance of D. Gravas, K. Giouras and C.G. Manos junior in conducting the field experiments and gathering geometric information relevant to the stone masonry bridges presented here as well as the help of the local people is gratefully acknowledged.

- To the memory of Ray W. Clough, Professor Emeritus of the University of California, at Berkeley, U.S.A.

REFERENCES

[1] Manos G.C., Nick Simos N. and Kozikopoulos E. (2016) “The Structural Performance of Stone-Masonry Bridges”, Chapter 4, "Structural Bridge Engineering", ISBN 978-953-51-2689-8, Print ISBN 978-953-51-2688-1, http://dx.doi.org/10.5772/64752.

[2] The stone masonry arch bridges of Greece, (2007) Center of environmental education Makrinitsas, Editor G. Grassos, ISBN: 978-960-98043-9-4, (in Greek). http://kpe-makrin.mag.sch.gr, e-mail: mail@kpe-makrin.mag.sch.gr

[3] Psimarni K., Georgopoulos A., Balodimos D.D. (2000), “Development of a Geographic Information System for the Traditional Bridges of Central Zagori,”, Report to the Municipality of Zagori, in Greek.

[4] Aoki T., et al, (2007), “Theoretical and Experimental Dynamic Analysis of Rakanji Stone Arch Bridge, Honyabakei, Oita, Japan,” 7th International Conference on Motion and Vibration Control, MOvIC 04.

[5] Sevim Barıs, et al., (2011), “Finite element model calibration effects on the earthquake response of masonry arch bridges,” Finite Elements in Analysis and Design, 47 (2011), 621–634

[6] Manos G.C. et al. (2015), “Field experiments for monitoring the dynamic soil-structure-foundation response of model structures at a Test Site” Journal of Structural Engineering, American Society of Civil Engineers, Special Issue “Field Testing of Bridges and Buildings, D4014012, Vol. 141, Issue 1, January 2015.

[7] Manos G.C. and Kozikopoulos E., (2015) “In-situ Measured Dynamic Response of the Bell Tower of Agios Gerasimos in Lixouri-Kefalonia, Greece and its Utilization of the Numerical Predections of its Earthquake Response”, COMPDYN 2015, Greece, 25–27 May 2015.

[8] Ozden Caglayan B., Kadir Ozakgul and Ovunc Tezer, (2012), “Assessment of a concrete arch bridge using static and dynamic load tests” Structural Engineering and Mechanics, Vol. 41, No. 1 (2012) 83-94

[9] Simos N. and. Manos G.C, (2013), “Numerical Analysis of Seismic Response of Natural Stone Arch Bridges-Field Observations and a Case Study,” COMPDYN 2013, http://www.eccomasproceedings.org/cs2013/

[10] Manos G.C. and Kozikopoulos E., (2015), "The dynamic and Earthquake Response of Basilica Churches in Kefalonia, Greece Including Soil-Foundation Deformability and Wall Detachment", COMPDYN 2015, Greece, 25–27 May 2015.

[11] Eurocode 8 - Design of structures for earthquake resistance - Part 2: Bridges, DRAFT No 3. European Committee for Standardization; 2004.

[12] Provisions of Greek Seismic Code 2000 , OASP, Athens, December 1999. Revisions of seismic zonation introduced in 2003.

[13] Paz. M. (1994) International Handbook of Earthquake Engineering: "Codes, Programs and Examples", edited by Mario Paz, Chapter 17, Greece by G.C. Manos, Chapman and Hall, ISBN 0-412-98211-0, 1994.

[14] Institute of Engineering Seismology and Earthquake Engineering (ITSAK), Data Base of Greek Earthquake Strong Motions".

[15] Manos G.C., Kotoulas L., Soulis V., Felekidou O. (2015), "Numerical Simulation of the Limit Non-Linear Behaviour of Unreinforced Masonry under In-plane State of Stress from Gravitational and Seismic Actions", COMPDYN 2015, Greece, 25–27 May 2015.

[16] Kiyono J., et al. (2012), "Seismic Assessment of Stone Arched Bridges," 15 WCEE, Lisboa, Portugal, 2012.

[17] Drosopoulos G.A., Stavroulakis G.E., Massalas C.V., (2006) "Limit analysis of a single span masonry bridge with unilateral frictional contact interfaces," Engineering Structures 28 (2006) 1864–1873

[18] Korompilias D., (2015), "Study of the inelastic behaviour of the Konitsa bridge using an inelastic model for masonry and applying strengthening methods," PhD Thesis, Univ. Of Patras, Greece, 2015 (in Greek).

[19] LS-DYNA - Version 9.71, Livermore Software Technology Corp. – LSTC, True-Grid - Version 2.3.4, XYZ Scientific Applications, Inc

[20] Papanastasiou D., (2001), "The Konitsa, Epirus NW Greece, July 26 (Ms = 5.4) and August 5, 1996, (Ms = 5.7) earthquakes sequence," Bull. Geol. Soc. Greece, XXXIV, 1555-1562.

[21] Spyrakos C. C., Maniatakis C. A. and Taflambas J., (2008), "Evaluation of near-source seismic records based on damage potential parameters Case study: Greece", Soil Dynamics and Earthquake Engineering 28 (2008) 738–753

[22] Non-linear Response to a Type of Seismic Input Motion, IAEA-TECDOC-1655-ISSN 1011-4289, June 2011,

[23] Manos G.C. (2011), "Consequences on the urban environment in Greece related to the recent intense earthquake activity", Int. Journal of Civil Eng. and Architecture, Dec., Volume 5, No. 12 (Serial No. 49), pp. 1065–1090.

[24] Galanakis D., Paschos P., et al. (2007) "Neotectonic Activity of Konitsa Area and the 1996 Earthquakes, Hellenic Journal of Geosciences, vol. 42, 57-64.

[25] Simos N. and Manos G.C., "Earthquake Vulnerability of Stone Arch Bridges using NonlinearFinite Elements and Measurements of Dynamic Characteristics," Engineering Structures, 2016 (submitted, in-review).

[26] Gianluca Ruocci, Antonino Quattrone, Luca Zanotti Fragonara, Rosario Ceravolo, Alessandro De Stefano, (2013) "Experimental Testing of a Masonry Arch Bridge Model Subject to

Increasing Level of Damage", IRIS, Chapter 6, Industrial Safety and Life Cycle Engineering, VCE Vienna Consulting Engineers, www.vce.at, ISBN 978-3-200-03179-1.

[27] Iraklis Milas, (2016), "Stone Bridges", Ethnos Travel Book, Ethnos Publications, ISBN:978-960-577-122-5 (in Grrek).